An Assessment of the Ability of Computational Fluid Dynamic Models to Predict Reactive Gas-Solid Flows in a Fluidized Bed

Schalk Cloete[1], Stein Tore Johansen[1] & Shahriar Amini[1*]

1) Flow Technology group, Department of Process Technology, SINTEF Materials and Chemistry, Trondheim, Norway

*Corresponding author. Email: shahriar.amini@sintef.no

Address: SINTEF Materials and Chemistry, Richard Birkelands Vei 3, 7034 Trondheim, Norway, Phone: +47 46639721

Keywords: Kinetic theory of granular flows; Fluidized bed; Chemical Looping Combustion; Reaction Kinetics; Grid Independence; Turbulence; Clusters

1. Abstract

Fine grid, two dimensional simulations of reactive gas-solid flows occurring in a fluidized bed reactor were carried out using an Eulerian multi-fluid kinetic theory of granular flow (KTGF) approach. The fuel reactor of a pilot scale Chemical Looping Combustion rig, operated in the bubbling fluidization regime at the Vienna University of Technology, was simulated. Grid dependence studies were carried out as well as sensitivity studies to the fuel inlet condition and the inclusion of gas phase turbulence. Simulations could not accurately reproduce the experimental trend for the case when highly reactive nickel oxide was used as the oxygen carrier material, but in general satisfactory quantitative agreement was observed. The failure to correctly capture the experimental trend was primarily attributed to the fine length-scales at the feed gas inlets not being adequately resolved even at the finest grid investigated. The trend quickly

worsened when coarser grids were used, indicating that the generality of the model is lost when grid dependence effects are present. A number of possible dimensional effects were also discussed. Subsequently, the model was used to successfully capture another experimental trend obtained with a much less reactive ilmenite oxygen carrier material. The model captured this trend correctly because the reaction was now limited by the reaction rate and not by species transfer to the large scale gas-emulsion interfaces. Results were therefore not as sensitive to the correct hydrodynamic modelling of the interface, especially near the gas inlets, and the model retained its generality over a wide range of operating conditions.

2. Introduction

Chemical Looping Combustion (CLC) is a promising technology for cost effective CO2 capture. CLC is a typical dual fluidized bed technology where a chemically active bed material, mostly a transition metal oxide, is circulated between two fluidized bed reactors within which it is exposed to different fluidizing gasses. The CLC fuel reactor reduces the oxygen carrier material with a fuel gas in the absence of air. This process produces an outlet stream of CO_2 and water vapour, enabling easy capturing of the CO_2. The reduced oxygen carrier material is then passed to an air reactor where it is oxidized by air to produce heat and a clean outlet stream of depleted air. More details about CLC can be found in [1].

Most of the research within CLC has been focused on particle development and reactivity testing of oxygen carriers in the laboratory or in small batchtype fluidized bed reactors [1]. Very limited works have been done with respect to understanding of the reactive multiphase flows in the CLC reactors. Small scale reactive CLC systems have been simulated before [2-3], but no proper validation of the approach has been completed. These studies have shown that CFD can give valuable insight into the system behaviour, especially with regards to the slippage of unreacted fuel gas past the bed material by means of bubbles. It has, however, not been established whether results from these simulations can be trusted to provide design and optimization guidelines. Simulation of reacting fluidized bed systems is very challenging and thorough validation will therefore be required before the models can be used for any practical purposes.

The selected modelling framework, known as the kinetic theory of granular flows (KTGF), is currently a well established method for simulating gas-particle systems. It has been proven to adequately predict the hydrodynamics in bubbling beds [4] and risers [5], but has not been validated towards the prediction of reactive gas-solid flows, mostly due to the lack of adequate experimental data. Recent work from the Vienna University of Technology [6], however, produced reliable conversion data for the fuel reactor of a 120 kW Chemical Looping Combustion (CLC) system over a range of operating conditions in the bubbling regime and the ability of CFD models to predict these flows can now be assessed.

The primary challenge in the simulation of gas-solid flows in fluidized beds is the formation of meso-scale particle structures within the domain. These structures take the form of gas bubbles in bubbling beds or particle clusters in risers. In order to accurately capture the physics, both from a hydrodynamic and reaction kinetic point of view, these meso-scale structures have to be resolved or adequately modelled. In

terms of particle structure modelling, research is under way to develop filtered drag laws [7-10] or even to represent the clusters as a separate phase [11]. These techniques are still in the development phase, however, and have not been thoroughly validated. Furthermore, research into appropriately filtering the reaction kinetic interaction is yet to commence. It is therefore estimated that a reliable filtered model for reactive gas solid flows will not be available for many years.

If a CFD based modelling approach is to be validated therefore, the finely resolved approach, based on proven models, will have to be taken. Computational limitations are such that only relatively small-scale systems can be simulated, and only if limited to 2D. Naturally, some degree of error will be introduced by simulating a 3D cylindrical reactive system on a 2D plane, but this cannot be avoided at present. Studies have also shown that a finely resolved 2D model can adequately predict the hydrodynamic behaviour of a 3D cylindrical system over a range of operating conditions [5].

This study is therefore undertaken on the hypothesis that reactive gas-solid flows occurring in a real CLC reactor can be adequately simulated with a finely resolved 2D planar model employing the kinetic theory of granular flows. Results from this study will indicate the degree to which this hypothesis is true and offer an indication as to how much further work is required towards a reliable predictive model for fluidized bed reactors.

3. List of Symbols

Main Symbol definitions:

Greek symbols:

α Volume fraction

ϕ_{gs} Interphase energy transfer (kg/m.s^3)

γ Dissipation rate (kg/m.s^3)

μ Viscosity (Pa.s)

Θ_s Granular temperature (m^2/s^2)

ρ Density (kg/m^2)

$\bar{\bar{\tau}}$ Stress tensor

$\vec{\upsilon}$ Velocity vector (m/s)

Regular symbols:

C	Molar concentration (mol/m^3)
D	Diffusivity (m^2/s)
d	Diameter (m)
$\vec{g}$	Gravity vector (m/s^2)
$\overline{\overline{I}}$	Identity tensor
$\vec{J}$	Diffusive flux
K_{sg}	Interphase momentum exchange coefficient
k	Diffusion coefficient (kg/m.s)
k	Reaction rate constant (mol^{1-n}m^{3n-2}/s)
M	Molar weight (kg/kmol)
N	Number of moles (mol)
p	Pressure (Pa)
R^H	Heterogeneous reaction rate (mol/m^{3}s)
S	Source term
s	Surface area fraction
Sh	Sherwood number
Sc	Schmidt number
Y	Species mass fraction

Sub- and superscript definitions:

Greek symbols:

Θ_s Granular temperature

$\vec{\upsilon}$ Momentum

Regular symbols:

c Core

g Gas

gs Gas-solid

i Species *i*

n Reaction order

t Turbulent

4. Simulations

4.1 Model equations

Within the Eulerian-granular framework, separate conservation equations are solved for the gas and the solids phases. Various constitutive models are subsequently required to close the equation system. A shortened outline will be given in this work, but the full equation system used is described in [12].

4.1.1 Conservation equations

The continuity equations for the two phases are solved as follows:

$$\frac{\partial}{\partial t}\left(\alpha_g \rho_g\right) + \nabla \cdot \left(\alpha_g \rho_g \vec{\upsilon}_g\right) = \alpha_g S_g \quad (1)$$

$$\frac{\partial}{\partial t}\left(\alpha_s \rho_s\right) + \nabla \cdot \left(\alpha_s \rho_s \vec{\upsilon}_s\right) = \alpha_s S_s \quad (2)$$

Source terms for both phases (right hand terms in equations (1) and (2)) are included to account for mass transfer due to heterogeneous chemical reactions.

Momentum conservation for the gas phase is written as

$$\frac{\partial}{\partial t}\left(\alpha_g \rho_g \vec{\upsilon}_g\right)+\nabla\cdot\left(\alpha_g \rho_g \vec{\upsilon}_g \vec{\upsilon}_g\right)=-\alpha_g \nabla p+\nabla\cdot\bar{\bar{\tau}}_g+\alpha_g \rho_g \vec{g}+K_{sg}\left(\vec{\upsilon}_s-\vec{\upsilon}_g\right)+S_g^{\vec{\upsilon}} \quad (3)$$

and for the solids as

$$\frac{\partial}{\partial t}\left(\alpha_s \rho_s \vec{\upsilon}_s\right)+\nabla\cdot\left(\alpha_s \rho_s \vec{\upsilon}_s \vec{\upsilon}_s\right)=-\alpha_s \nabla p-\nabla p_s+\nabla\cdot\bar{\bar{\tau}}_s+\alpha_s \rho_s \vec{g}+K_{gs}\left(\vec{\upsilon}_g-\vec{\upsilon}_s\right)+S_s^{\vec{\upsilon}} \quad (4)$$

Momentum sources due to mass transfer from heterogeneous reactions (final terms in equations (3) and (4)) are included.

Species are also conserved for each individual phase.

$$\frac{\partial}{\partial t}\left(\alpha_g \rho_g Y_{g,i}\right)+\nabla\cdot\left(\alpha_g \rho_g \vec{\upsilon}_g Y_{g,i}\right)=\nabla\cdot\alpha_g \vec{J}_{g,i}+\alpha_g S_{g,i} \quad (5)$$

$$\frac{\partial}{\partial t}\left(\alpha_s \rho_s Y_{s,i}\right)+\nabla\cdot\left(\alpha_s \rho_s \vec{\upsilon}_s Y_{s,i}\right)=\nabla\cdot\alpha_s \vec{J}_{s,i}+\alpha_s S_{s,i} \quad (6)$$

Interphase species transfer will be considered via additional source terms (final terms in equations (5) and (6)).

No energy conservation was simulated as isothermal flow was assumed. The simulated reaction is only moderately endothermic and the experimental conditions were carefully controlled to operate the reactor within ±6 K from the set point [6]. The continuous circulation of solid materials and the excellent mixing achieved in fluidized beds should therefore ensure negligible spatial and temporal temperature variations within the reactor, making the isothermal assumption a valid one.

4.1.2 Closures

4.1.2.1 Drag

Gas-particle momentum exchange was modelled according to Gidaspow [13]. Other drag correlations [14-15] but only negligible differences between these models were found. This is a result of the rather dense system being simulated with well resolved particle structures. The primary interphase momentum exchange is therefore simulated directly on the large scale interface of these structures as shown in [5].

4.1.2.2 Gas phase turbulence

The possible effect of including gas phase turbulence was also evaluated by calculating the turbulent viscosity according to Smagorinsky [16] with a model constant of 0.2. The value of this constant is recommended to be increased for 2D simulations according to Murakami *et al.* [17] who increased in from 0.1 in 3D to 0.15 in 2D. Another study [18] found the best fit for 2D LES to be achieved with a Smagorinsky constant as high as 0.75. Clearly then, there exists significant uncertainty in the correct value of this constant, but the value of 0.2 was selected to be close to the recommendation from Murakami *et al.* [17] since their system more closely resembled the present one.

It is acknowledged that, due to the inherently 3D nature of turbulent vortices, 2D LES is fundamentally limited. The inclusion of a 2D LES in the current study is only implemented as a measure to simulate the increased diffusive species transport that was found to be important in the system investigated. Turbulent diffusion of species was simulated based on the calculated turbulent viscosity as follows:

$$\vec{J}_i = -\left(\rho D_i + \frac{\mu_t}{Sc_t} \right) \nabla Y_i \qquad (7)$$

The turbulent Schmidt number $\left(Sc_t\right)$ was taken to be 0.7.

4.1.2.3 Kinetic theory of granular flows

In the KTGF analogy, the random motion of granular particles is likened to that of gas molecules where the kinetic theory of gasses is applied. This analogy allows the determination of fluid properties for the particulate phase by accounting for the inelasticity of the particles. The granular temperature is a measure of the energy contained in these random particle motions and is written in conservation form as follows:

$$\frac{3}{2}\left[\frac{\partial}{\partial t}\left(\alpha_s \rho_s \Theta_s\right)+\nabla\cdot\left(\alpha_s \rho_s \vec{\upsilon}_s \Theta_s\right)\right]=\left(-p_s\bar{\bar{I}}+\bar{\bar{\tau}}_s\right):\nabla\vec{\upsilon}_s+\nabla\cdot\left(k_{\Theta_s}\nabla\Theta_s\right)-\gamma_{\Theta_s}+\phi_{gs} \quad (8)$$

The diffusion coefficient in the granular conductivity term was modelled according to Syamlal and O'Brian [14], the collisional dissipation of kinetic energy according to Lun et al. [19] and the interphase energy exchange according to Gidaspow et al. [13].

The granular temperature is subsequently used to calculate values of the solids viscosity which is used in the solids stress tensor. Bulk and shear viscosities occur due to particle translation and collision in the solids phase. The bulk viscosity is calculated following Lun et al. [19], while the kinetic, collisional and frictional components of the shear viscosity is modelled according to Gidaspow et al. [13], Syamlal and O'Brian [14] and Schaeffer [20] respectively.

Within the KTGF analogy, a solids pressure is also defined to be used in equation (8) as well as in equation (4) and is calculated according to Lun *et al.* [19]. The radial distribution function indicating the average distance between particles is used throughout the KTGF and is calculated according to Ogawa et al. [21].

4.1.2.4 Heterogeneous reaction rate

Reaction kinetics was implemented by using the shrinking core methodology [22]. For the particular particle simulated in this study, the shrinking core model was applied to small spherical grains within the particle. Based on the particle manufacturing process, it was assumed that the particle consists of pure grains of reactive material surrounded by grains of non-reactive material.

The reaction simulated in this study is the reduction of NiO by methane. The natural gas used in the experiments contained 98.7 vol% methane [6], making this a valid assumption.

$$4NiO + CH_4 \rightarrow 4Ni + CO_2 + 2H_2O$$

The assumption was made that the process was reaction rate controlled. Thus [22]:

$$-\frac{dN_{CH_4}}{dt} = \pi d_c^2 k C_{CH_4}^n \quad (9)$$

The possible mass transfer limitation can be checked with the simple case of a sphere in a stationary and infinite medium. If the medium is not moving, mass transfer would occur exclusively by diffusion and be at a minimum. The mass transfer coefficient can be approximated from $Sh = 2$. For a particle diameter of 120 µm and a diffusivity of 0.9 cm^2/s, the mass transfer coefficient returned would be 1.5 m/s. The rate constant for the reduction reaction between the specific oxygen carrier material used in the experimental studies and methane was determined by Abad et al. [23] as the following:

$$k = 2.5e^{(-70000/RT)} \quad (10)$$

At a reaction temperature of 1173K, the rate constant is 0.0019 m/s which is substantially lower than the mass transfer limitation. However, the reaction rate constant was calculated on smaller grains (10 µm) residing inside of the particle and not on the particle itself. The reaction rate was calculated only on grains of pure NiO within the particle [23]. For the particular particle used, the surface area presented by these pure NiO grains represents a fraction of 0.2066 of the surface area presented by all the grains in the particle. It would therefore be more accurate to check the volumetric reaction rates for the mass transfer limitation on the particle and reaction rate limitation in the pure NiO grains. The volumetric reaction rate can be expressed as follows:

$$-\frac{1}{V}\frac{dN_{CH_4}}{dt} = \frac{6}{d_s} s_{NiO} k \alpha_s C_{CH_4}^n \quad (11)$$

At a constant volume fraction, reaction order and methane concentration, the ratio of the mass transfer controlled rate and the reaction controlled rate calculated from equation (11) would be $\left(1.5/120\right)/\left(0.0019\times 0.2066/10\right)=318.4$. It is therefore clear that the reaction rate would be more than two orders of magnitude faster if it was controlled by mass diffusion to the particle. I fact, in the TGA experiments completed by Abad *et al.* [23] showed that mass transfer is so fast that it is even safe to assume that mass transfer to all the grains inside the particle is not limiting. This was established by conducting experiments with different sizes of particles to find that the reaction rate was not affected by particle diameter.

Following this analysis, the reaction rate calculations can safely be conducted on the assumption that reaction rate on the NiO grains inside the particle is controlling. The rate per unit volume reaction description implemented into the flow solver is provided below:

$$R^H = -\frac{1}{V}\frac{dN_{CH_4}}{dt} = \frac{6}{d_s} s_{NiO}\alpha_s x_{NiO}^{2/3} k\left(\frac{x_{CH_4}\rho_g}{M_{CH_4}}\right)^n \qquad (12)$$

The calculated reaction rate constant is to be used in Equation (12) with a grain diameter $d_s = 10\ \mu\text{m}$ and a reaction order $n = 0.6$. The mass fraction of NiO $\left(x_{NiO}\right)$ is included to describe the reduction of available surface area as the reaction proceeds and the unreacted core of NiO shrinks.

A full description of how the calculated heterogeneous reaction rate is implemented to determine the source terms used in the conservation equations can be found in [12].

4.2 Geometry and boundary conditions

The reactor to be simulated is 0.16 m in diameter and 3 m in height [6]. The lower loop seal connecting this reactor (fuel reactor) to the air reactor forms part of the reactor body and thereby extends the reactor length downwards. A graphical representation of this setup can be found in Pröll et al. [6]. Fuel gas is injected by means of three nozzles (I.D. 10 mm) equally spaced around the circumference of the reactor and injecting the gas downwards at an angle of 45^{o} at a location of half a radius inwards.

The simulated reactor domain is shown in Figure 1.

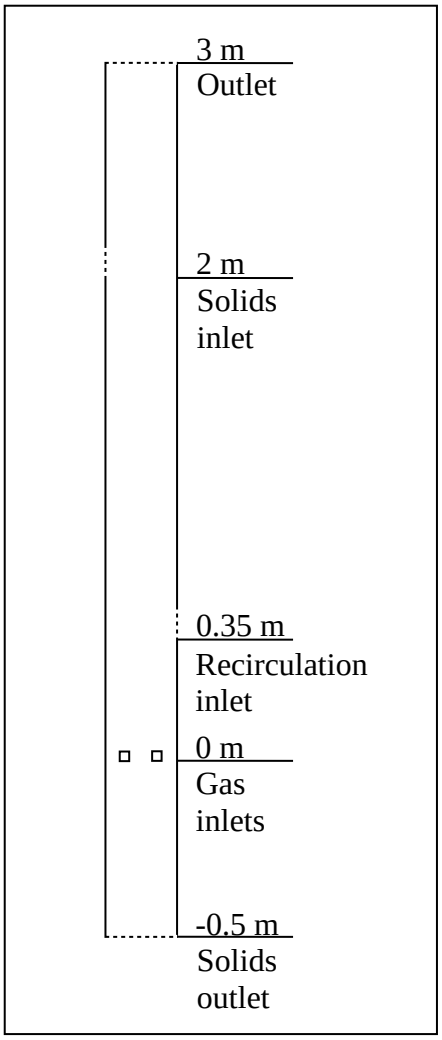

Figure 1: The 2D planar geometry simulated in the present study.

As shown in Figure 1, the solids inlet is located quite high up in the reactor, while the solids outlet is located right at the bottom. The 0.5 m extension between the gas inlets and the solids outlet is specified to simulate the loop seal that will transport the solids to the air reactor. Both these boundary conditions were specified as velocity inlets, the inlet given a positive velocity and the outlet a negative velocity, according to the specified experiment. These two inlets were specified so that the exact mass of solids being injected via the inlet would be extracted via the outlet.

A recirculation inlet for the solids is located closer to the gas inlets. A variable velocity inlet was used so as to re-inject all the solids that exited at the outlet (top of the domain). In the experimental rig, this recirculation is accomplished by a cyclone and a recirculation loop. The reintroduction of recycled solids will therefore not be instantaneous as in the simulation, but this model approximation should still be reasonable.

The gas is injected via one or two 5x5 mm^2 regions designated to contain mass and momentum sources. These mass and momentum sources were set to reflect the mass flow rate and velocity of the gas being injected by the three experimental injection nozzles for each individual experiment. The gas exits at the top outlet which is defined as a pressure outlet at atmospheric pressure.

A simple no-slip wall boundary condition was set for the gas phase, while the Johnson and Jackson [24] boundary conditions were used for the granular phase. The specularity coefficient and particle wall restitution coefficient required by the Johnson and Jackson boundary condition were set to 0.1 and 0.9 respectively. Of these two parameters, the specularity coefficient is known to have a large influence on riser simulations where the flow is dilute and the near wall velocity is likely to be high, but for the denser flows simulated in the present study, the wall boundary condition is expected to have a less pronounced influence.

4.3 Solver settings

The commercial CFD package, FLUENT 12.1 was used as the flow solver to carry out the simulations. The phase-coupled SIMPLE algorithm [25] was selected for pressure-velocity coupling, while the QUICK scheme [26] was employed for discretization of all remaining equations. 2^{nd} order implicit temporal discretization was used.

4.4 Problem setup summary

Table 1: Summary of model settings used in the simulations.

	Gas	Solids
Temperature	Isothermal – 1173K	Isothermal – 1173K
Density	Volume weighted average of species density at 1173K	3200 kg/m^3
Viscosity	Mass weighted average of species viscosity at 1173K	KTGF
Diffusivity	0.9 cm^2/s	1e-6 cm^2/s (very low number)
Particle diameter		120 μm
Particle-particle restitution		0.9
Particle-wall restitution		0.9
Specularity coefficient		0.1
Particle sphericity		0.99 (assumed spherical)
Maximum packing limit		0.63
Fuel power	54.7 – 139 kW	
Lower heating value of fuel	48.8 MW/kg	
Inlet composition	100% Methane	

The gas feed rate for each simulation was calculated simply by dividing the required fuel power with the lower heating value of the fuel. The resulting mass flow rate was adjusted for 2D to maintain the same superficial velocity in both cases by multiplying with the ratio of the cross sectional areas of the two geometries presented $\left(4/\pi D\right)$. Solids mass flow rates and holdup was found from Pröll *et al.* [6] and subjected to the same 2D adjustment. A summary of the resulting boundary conditions for the five cases considered in the present study is given in Table 2.

Table 2: Flow boundary condition and solids holdup specifications for the five cases investigated in the present study.

Case (kW)	Gas flow rate (kg/s)	Solids flow rate (kg/s)	Solids holdup above injection points (kg)
54.7	0.00892	2.698	152.0
79.2	0.01292	5.371	165.5
101.0	0.01647	8.833	174.3
121.0	0.01973	10.663	173.5
139.0	0.02267	12.812	174.3

4.5 Operation and data extraction

The solution was initialized with a volume fraction in the reactor section above the inlets that would constitute the correct mass of particles in the reactor according to the measurements in [6]. Additional solids were patched in below the gas inlets at maximum packing. The simulation was then run until quasi-steady stat behaviour was displayed by the average solids velocity and the total reaction rate in the reactor. Data collection was then commenced for a minimum of 15s simulation time. This time was tested to be sufficient to adequately represent the averaged behaviour of the system.

The mass flow of methane across the outlet was measured and averaged over the 15s flow time in order to get the overall methane conversion achieved in the reactor. Time statistics were also collected for this period in order to get time-averaged axial plots of pressure and species concentration.

5. Results and discussion

Four sets of numerical experiments were performed. The first three of these included a grid independence study, a study of different inlet configurations and an investigation into the effect of including gas phase turbulence. These three studies focussed only on the lowest and highest fuel power cases (57.4 and 139 kW). Finally, five numerical simulations at different fuel feed rates were run and compared to experimental results.

5.1 Numerical experiment 1: Grid independence study

The lowest and highest fuel power cases were run on three different grid sizes. Results in terms of methane conversion are shown in Table 3.

Table 3: Simulated reactor performance on different grid sizes.

Grid size (mm)	Unconverted methane (%)		Equivalent reactor height (m)	
	57.4 kW	139 kW	57.4 kW	139 kW
1.8	2.48	3.60	1.41 (0.0%)	3.00 (0.0%)
2.5	1.40	3.55	1.51 (+7.1%)	3.01 (+0.3%)
3.5	0.40	4.89	1.60 (+13.5%)	2.74 (-8.7%)
5.0	0.32	6.24	1.61 (+14.2%)	2.50 (-16.7%)

The measure 'equivalent reactor height' in Table 3 is given in order to linearize the 'unconverted methane' performance measure. Reaction rate is dependent on the amount of methane available and will thus reduce as the methane is depleted towards the upper regions of the reactor. The methane converted will therefore change in a non-linear way along the height of the reactor. The degree of non-linearity will be primarily dependent on the reaction order where a 0^{th} order reaction will approach linear reactant decay while the decay with a first order reaction will be strongly exponential. The current reaction order is 0.6, implying that some degree of non-linearity will be present. This can be seen in Figure 4 presented later. In order to attain a linearized measure for reactor performance, a curve fit was done to the upper part of the methane conversion curve attained from the highest resolution runs (1.8 mm grid size) as shown in Figure 2. These curves can then be used to find the reactor height corresponding to the final degree of methane conversion achieved in any specific run. Reactor height is a linear, easily visualized parameter and should aid in the interpretation of results. In order to easily compare between cases, the percentage deviation from a reference reactor length is also given.

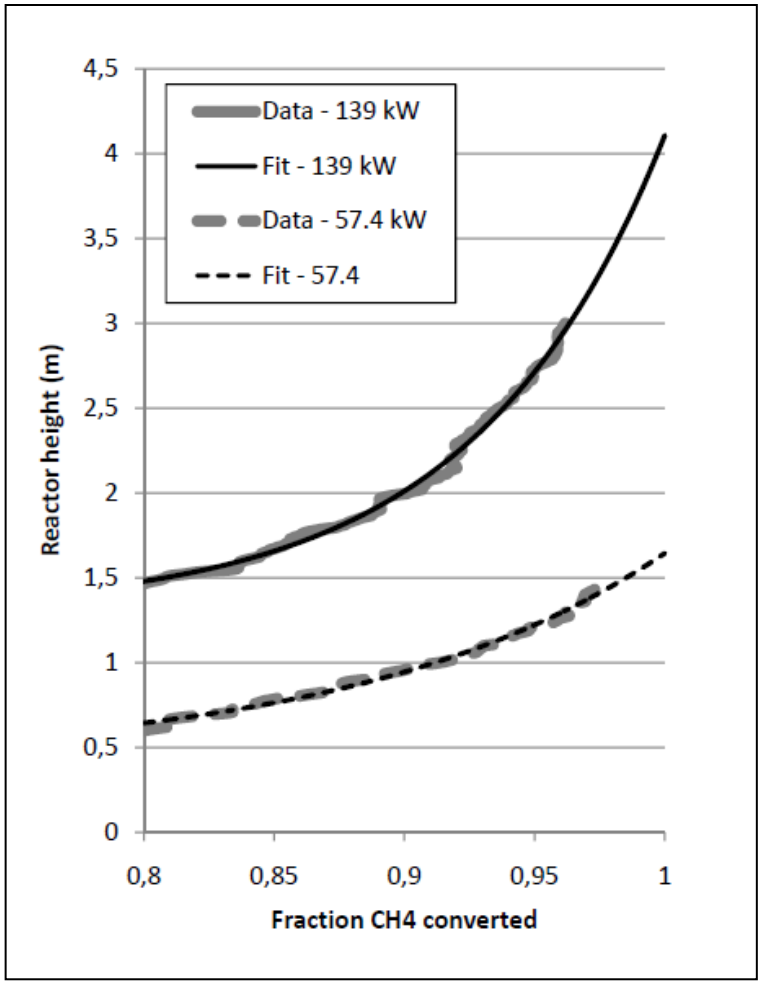

Figure 2: Curve fit to the upper part of the methane conversion curve for the two fuel power cases considered.

When looking at the simulated reactor performance in Table 3, two distinctions can immediately be made. Firstly, grid independence is only achieved for the 139 kW case, while the solution continues to change in the 57 kW case. Secondly, the effect of refining the grid has opposite effects in the two cases simulated; increasing the methane conversion in the 139 kW case and decreasing it in the 57.4 kW case. This is the first indication that grid dependence effects caused by particle structures in the bed may be decreasing the fidelity of the model.

These two effects will be discussed in more detail below:

5.1.1 The 139 kW case

Grid independent behaviour in fluidized bed reactors is primarily dependent on the resolution of particle structures (clusters or bubbles) inside the domain. A better understanding can therefore be gained by studying the distribution of the solid volume fractions resolved on the different grids as shown in Figure 3.

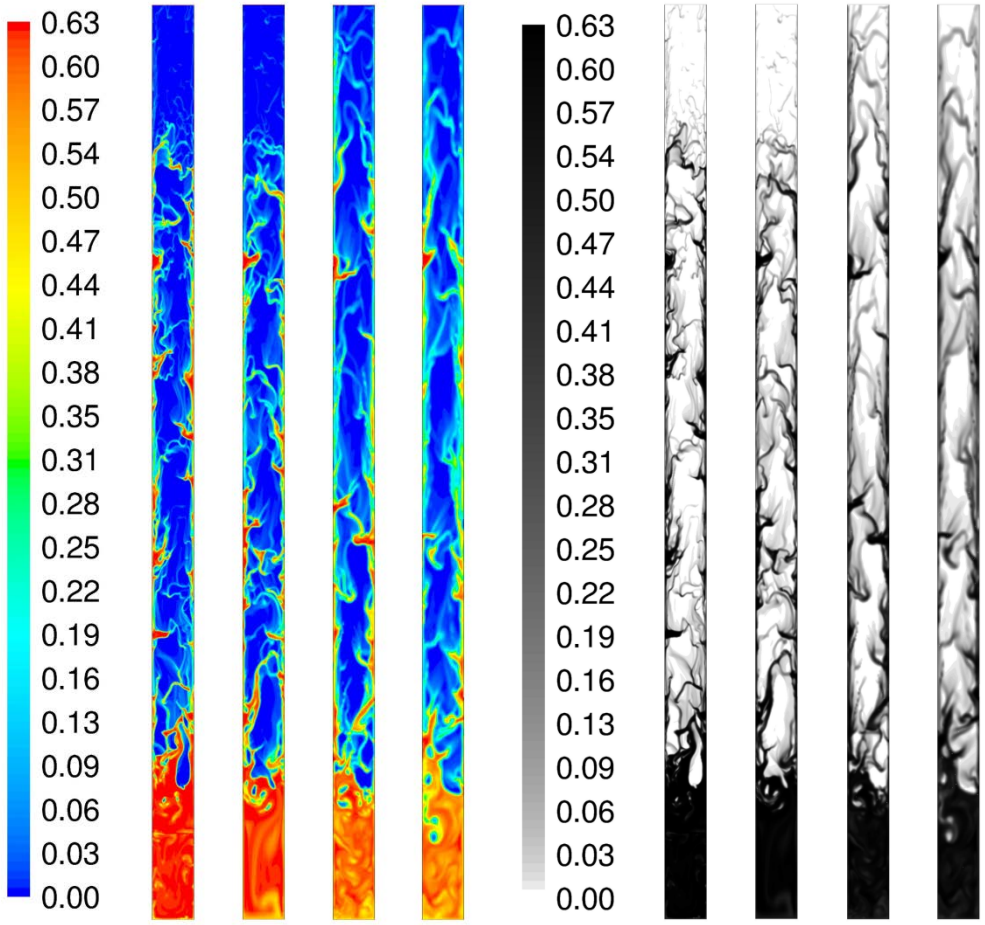

Figure 3: Instantaneous solid volume fraction contours for the three different grid sizes investigated. Grid size increases from left to right.

Two competing effects influence the reaction kinetic interaction between phases when solved on different grid sizes. One of these was identified in a cluster resolution study for risers [12]. It was concluded that coarser meshes, i.e. poorer cluster resolution, increased the reaction rate since the separation between the fuel rich gaseous regions and the fuel depleted dense regions was less distinct due to numerical diffusion. This increased the contact between fuel rich gas and solid particles and resulted in generally higher reaction rates. From Figure 3, it is clear that this reduction in separation sharpness between phases is present in this case also, but Table 3 shows that, contrary to the findings of [12], the reaction rate is actually reduced by coarsening the grid.

The reason for this surprising trend can also be deduced from Figure 3. It is clear that, when comparing the 1.8 and 5 mm meshes, the surface area between the resolved cluster phase and the gas phase is much larger for the finer mesh since much finer structures are resolved. Another probable influence is the dispersive effect of these well resolved clusters. Well resolved solid structures constantly obstruct the central channel and thereby redirect the flow. This increases the distance that the gas has to travel

through the reactor and represents a beneficial mixing mechanism. Non-resolved turbulent diffusion of methane to the large scale interfaces might also play a substantial role in the overall reaction rate. No turbulence model was included in this grid independence study, so turbulent diffusion was not modelled. All three of these effects will serve to decrease the reaction rate with an increase in cell size.

When looking at the axial profiles of methane conversion in Figure 4, it can be seen that the first mechanism (increased gas-solid contact and faster reaction rates due to smeared out clusters) is dominant in the lower reactor regions, while the second mechanism (decreased gas-solid contact area and slower reaction rates due to poorly defined clusters and non-resolved turbulent diffusion) starts to dominate in the upper regions. This can be identified by the amount of methane converted on the coarse grid being highest in the lower regions and then switching to being lowest in the upper regions.

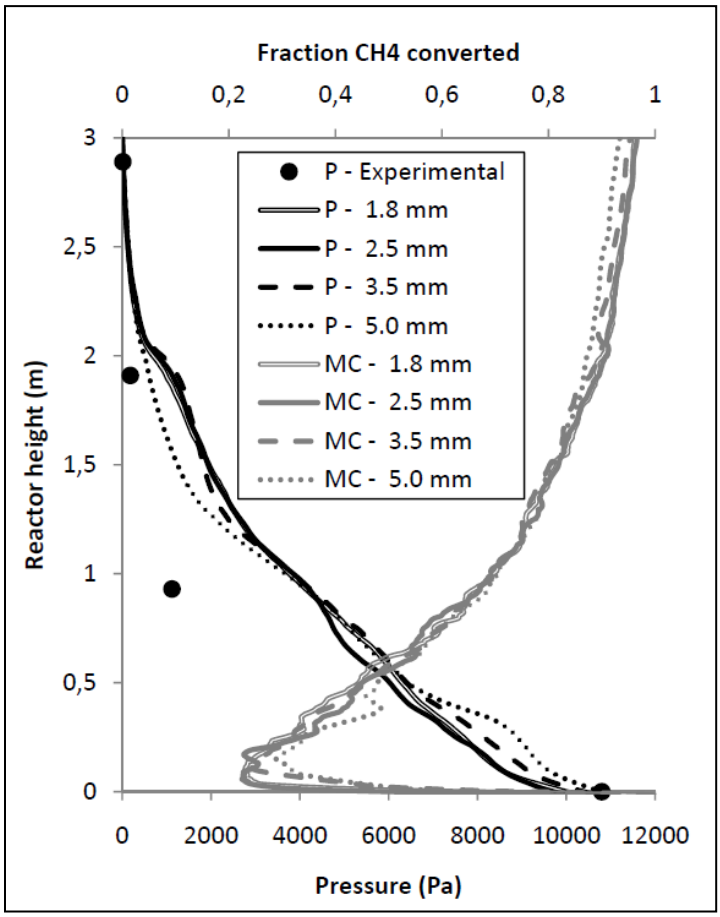

Figure 4: Time averaged pressure (P) and methane conversion (MC) variation along the height of the reactor in the 139 kW run solved on different grid sizes.

Even though the resolved structures in Figure 3 show some large qualitative differences, Table 3 and Figure 4 show only a moderate quantitative influence on the methane conversion. This is an indication that the two competing effects described above are of similar importance and can result in seemingly grid

independent behaviour before it truly is achieved. The grid independence achieved between the grid sizes of 1.8 mm and 2.5 mm seems to be authentic, however, since the axial methane conversion profiles returned by these two simulations match all the way through the length of the riser.

It is also interesting to look at the grid dependence behaviour of the most important hydrodynamic quantity: the pressure drop. Figure 4 shows this quantity to achieve satisfactory grid independence for grids of 0.0035 m and smaller. It is also clear that the bed expansion is over-predicted by the model. This is to be expected when simulating a 3D cylindrical system on a 2D plane. The dense solids regions near to the wall will weigh more in a 3D cylindrical system that they do on a 2D plane. This implies that, under a core-annular flow structure, more solids mass can be accommodated per bed height in a 3D cylindrical system than in a 2D planar system.

5.1.2 The 57.4 kW case

Grid independence is never achieved in the 57.4 kW case. This is somewhat surprising since this case lies well within the bubbling fluidization regime. The bubble structures formed in these slower beds are generally larger and therefore easier to capture on coarser grids than the cluster structures formed in faster beds. In this case, however, the inlet conditions used in the experiment occur on very small length scales. The source term by which the gas is injected was implemented on a single cell when the 5 mm grid was used. It is evident that this inlet region would need to be discretized into a substantially larger number of control volumes in order to adequately capture the necessary flow details. This inlet region is also a highly reactive area of the reactor since the highly concentrated fuel gas is contacted with a dense mass of solids. Any grid dependent behaviour in this area will therefore be strongly exaggerated. An insufficiently fine grid will over-predict the reaction rate by not simulating a sufficiently sharp boundary between the concentrated gas and the dense solids.

Yet, when looking at Table 3, the impact of the grid on simulated reactor performance seems to be relatively small over the range investigated. This is misleading though since it turns out that the two opposing grid dependence mechanisms described earlier are more balanced in the 57.4 kW case. Figure 5 illustrates this by showing a big effect of the first mechanism (increased gas-solid contact and faster reaction rates due to smeared out clusters) in the lower reactor regions, and a subsequent cancelling out of this effect by the second mechanism (decreased gas-solid contact area and slower reaction rates due to poorly defined clusters and non-resolved turbulent diffusion) towards the upper reaction regions.

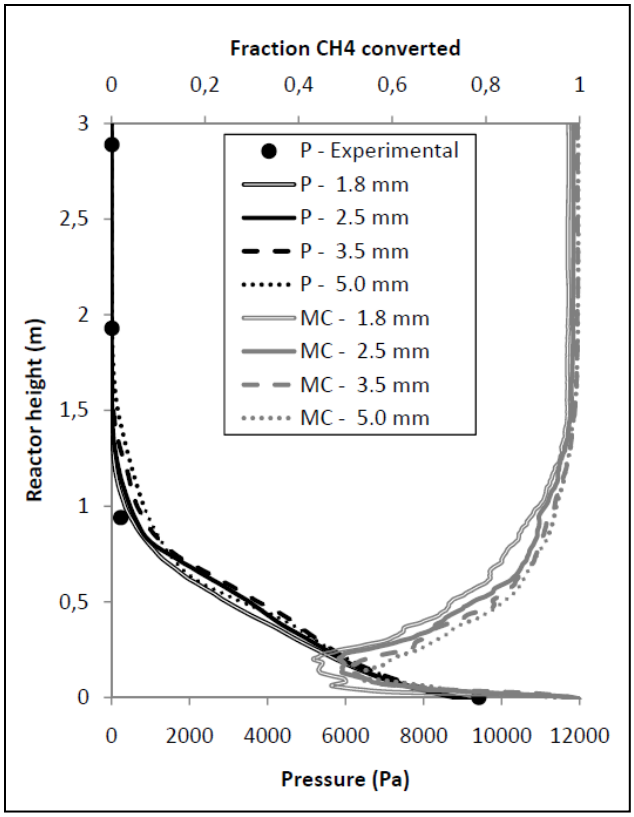

Figure 5: Time averaged pressure (P) and methane conversion (MC) variation along the height of the reactor in the 57.4 kW run solved on different grid sizes.

The reason for the rather strong grid dependence shown in this case (observed in the lower regions of Figure 5) is that it contains much larger particle concentrations around the inlet region. The high gas injection rate of the 139 kW case frequently creates a pocket of gas around the injection point so that there is no need for a high solids volume fraction gradients to be resolved in this region. In the 57.4 kW case, however, the injection point is often swamped by falling solids, thereby requiring the resolution of very sharp solids volume fraction gradients.

The pressure drop again shows adequate grid independence behaviour, especially for the two finest cases. It is also interesting to note the coupling between the pressure drop (hydrodynamics) and the methane conversion (reaction kinetics) in this figure. The reaction simulated in this study increases the gas volume by a factor of 3 when it occurs. More reaction will therefore imply more fluidizing gas. It is interesting to see that the bed height is higher on the 5 mm and 3.5 mm grids where more reaction takes place. This additional interaction makes it difficult to pinpoint with any certainty whether hydrodynamic grid independence is in fact achieved. The comparison to experimental results, however, is much better in this case because the degree of radial solids segregation is much lower than that shown by the 139 kW case.

5.2 Numerical experiment 2: Inlet effects

Computational expenses required to solve the case with 1.8 mm grid cells was already prohibitively expensive, requiring almost one month of simulation time on 8 processors. The remainder of the study will therefore be carried out using the 2.5 mm grid spacing.

The method of injection used in the experimental setup against which comparisons are made [6] introduces a large amount of uncertainty to the simulation results. Experimentally, the fuel gas is injected from three 10 mm ID injection nozzles equally spaced, half a radius from the reactor centreline. Firstly, these injections are highly localized, the area over which the three injections are made being just 1.17% of the reactor cross sectional area. Simulating reactive simulations in 3D on such small lengthscales will remain computationally impractical for many years to come. The 2D approximations used in the present study, even when only one inlet is used, inject the gas over a 3 times larger area in relation to the cross sectional area of the reactor. The grid independence study reported in the previous section has shown that the lengthscales involved in the injection zone may be too small to properly resolve the local transport phenomena even in 2D.

Secondly, the geometrical arrangement of the injection points in the experiment is not easily translated from a 3D cylindrical to a 2D planar geometry. Therefore, two options were evaluated here: a single inlet, as would be seen if a 2D slice were taken through one of the inlets and the reactor centre point, and 2 symmetrical inlets to simulate the symmetry on the experimental injection setup. The results for these two simulations competed for both the 139 kW and the 57.4 kW cases are presented in Table 4.

Table 4: Simulated reactor performance with the two different inlet conditions.

Number of inlets	Unconverted methane (%)		Equivalent reactor height (m)	
	57.4 kW	139 kW	57.4 kW	139 kW
1	1.40	3.55	1.51 (+0.0%)	3.01 (+0.0%)
2	0.66	3.25	1.58 (+4.6%)	3.08 (+2.3%)

As expected, the effect is larger in the 57.4 kW case where the inlet effects play a major role. When two injections are used, the gas is being injected in a more dispersed manner increasing the bubble-emulsion contact area in the high reaction zone close to the inlets. For the 139 kW case, the injection rate is strong enough to often create a central pocket of gas into which both gas injection points can inject the fuel gas. The conversion given by the two different inlet setups is therefore very similar.

5.3 Numerical experiment 3: Gas phase turbulence

The inclusion of gas phase turbulence was shown to be insignificant on the hydrodynamics of well resolved 2D riser flows [27] and a similar conclusion is expected here. Gas phase turbulence could have a significant effect on species diffusion in the gas phase though. In the present simulation setup, the reaction rate is very high and gas reacts almost instantaneously when brought into contact with the dense emulsion phase. Increased species diffusion would increase the diffusive transport of methane to

this reactive interface, thereby increasing the reaction rate. Simulation results for this numerical experiment are given in Table 5.

Table 5: Simulated reactor performance with and without the inclusion of gas phase turbulence.

Gas phase turbulence	Unconverted methane (%)		Equivalent reactor height (m)	
	57.4 kW	139 kW	57.4 kW	139 kW
No	1.40	3.55	1.51 (+0.0%)	3.01 (+0.0%)
Yes	1.17	2.69	1.53 (+1.3%)	3.24 (+7.6%)

In both cases, the inclusion of gas phase turbulence caused an increase in the global reaction rate. The greater species diffusion caused by the inclusion of turbulence therefore seems to have a significant, albeit not large, effect on the global reaction rate. This can be attributed to the small cell size causing the majority of cells to contain a low modelled turbulent viscosity in the same order as the molecular viscosity. As expected, the 139 kW shows a greater impact of the inclusion of turbulence due to the higher flow velocities present in this case.

Since gas phase turbulence was found to be a significant factor, it can now be tested whether the inclusion of gas phase turbulence can reduce the impact of the second grid dependence effect (decreased gas-solid contact area and slower reaction rates due to poorly defined clusters and non-resolved turbulent diffusion) discussed in section 5.1.1. The two coarser grid resolutions were therefore repeated with the inclusion of gas phase turbulence.

Table 6: Simulated reactor performance for the 139 kW case with and without gas phase turbulence on different grids.

Grid size	Unconverted methane (%)		Equivalent reactor height (m)	
	No turbulence	Turbulence	No turbulence	Turbulence
2.5	3.55	2.69	3.01 (+0.0%)	3.24 (+0.0%)
3.5	4.89	3.05	2.74 (-9.0%)	3.15 (-2.8%)
5.0	6.24	4.31	2.50 (-16.9%)	2.85 (-12.0%)

Table 6 shows that grid dependence between the 2.5 and 3.5 mm grids has decreased markedly, bringing the difference down from 9.0% to 2.8% when measured on the equivalent reactor height scale. This confirms that sub-grid gas-phase turbulence is indeed an important factor to be accounted for. An equivalent improvement is not reflected in the 5 mm case, however, despite the significantly larger turbulent viscosity that is simulated on the larger grid employed here. This is an indication that the physics of the system is in the process of being lost due to inadequate particle structure resolution. The substantial reduction in the large-scale gas-solid interfacial area observed in Figure 3 now starts to dominate despite the improved diffusive reactant transport.

5.4 The influence of variations in fuel power

The total degree of methane conversion achieved in this reactor is the only reliable set of reactive CLC data available in the literature against which comparisons can be made. The fuel power (mass flow rate of methane) into the reactor was varied and the degree of methane conversion was measured to show a somewhat surprising trend of greater conversion at higher fuel powers. The simulations were completed on the 2.5 mm grid with only one gas injection point and the gas-phase turbulence model activated.

As shown in Figure 6, the model is not in qualitative agreement with the experiments, showing the more intuitive trend of greater fuel conversion at lower fuel powers. Quantitatively, however, the results seem to be in the correct order, especially towards the higher fuel powers. This is a positive indication that TGA experiments performed on single particles can be used in flow models to describe the reactive behaviour of the full flow system.

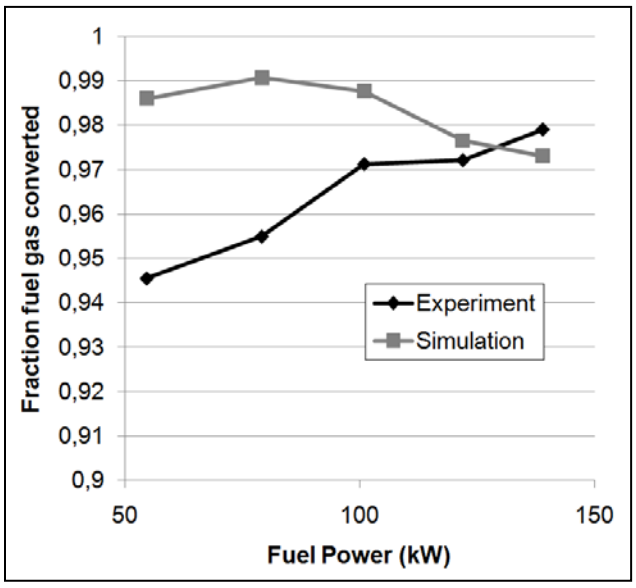

Figure 6: Comparison between experimental measurements [6] and numerical prediction of gas conversion over five different fuel powers.

5.4.1 Discussion of the experimental results

In the experiments, an increase in the fuel power of the system actually increased the degree of fuel conversion despite the lower gas residence time. This was attributed to the extra bed expansion at higher fuel powers [6], but according to axial pressure profile measurements, this extra bed expansion was not all that significant. The residence time of the gas in the bed region would still be significantly shorter at higher fuel powers, implying that some other significant mechanisms have to be considered in addition.

The primary of these effects is expected to be the concentrated fuel injection sources. Especially at lower gas injection rates, these point injection sources would create large bubbles already in the lower regions of the reactor, thereby reducing the contact between the fuel and the particles. If a standard distributor plate was used to inject the gas, it is highly likely that the reaction rate at low gas injection rates would be much higher due to the greater contact between the dispersedly injected fuel gas and the solid particles.

In another set of experiments performed in the same experimental rig where much less reactive, natural materials were used as the oxygen carrier [28], the expected, opposite trend of better conversion at lower fuel power was observed. This is a further indication of the large impact of the initial bubble formation facilitated by the point injection sources. When materials with low reactivity are used, the global reactor conversion is likely to be limited by the reaction rate. With highly reactive materials, such as used in the present study however, the global reaction rate is limited by the species transfer to the bubble-emulsion interface where the reaction is virtually instantaneous. The reactive behaviour of such a system therefore depends primarily on the hydrodynamics and in this case, the gas injection mechanism especially.

A second reason for the counterintuitive experimental conversion trend shown in Figure 6 could be the increased gas-solid contact in the splash region and the freeboard. According to standard flow regime diagrams [29], all of the present cases are still operated in the bubbling fluidized bed regime, the highest fuel powers being close to but not yet inside the turbulent fluidization regime. There should therefore be an insignificant amount of solids entrainment and the freeboard region should be very lean in particles. When such a highly reactive oxygen carrier is used, however, even particle lean regions can have a substantial influence on the global conversion rate.

5.4.2 Discussion of the simulation results

The inadequate capturing of this enhanced bubble formation effect at the inlet is considered to be the primary reason for the discrepancy between the model and experimental results at lower fuel powers. As mentioned previously, the clear phase separation is probably not adequately captured even on the fine grids used in the present study. This leads to over-predictions of gas-solid contact and therefore reaction rate in this crucial region. The grid independence study conducted suggested that the conversion in the low fuel power case would continue to decrease as the grid was refined beyond the size permitted by computational constraints. It is therefore possible that additional grid refinement alone would correct the erroneous trend shown in Figure 6, but unfortunately it is presently impossible to confirm this notion.

The incorrect trend in Figure 6 stresses the importance of ensuring grid independence in reactive fluidized bed simulations. The two conflicting effects discussed in section 5.1.1 vary in strength at different operating conditions and thereby negates the generality of the model on coarser grids. Simulations performed on coarser grids (Table 3) show that the trend Figure 6 would become significantly worse if it were reproduced on an even coarser grid.

A second possible reason for general reaction rate over-predictions in the simulations could be the formulation of the two-fluid model not producing sufficiently lean bubbles. The simulation almost

exclusively resolves bubbles containing more than 1% of solids. Transient experimental measurements of void fraction in bubbling beds [30] show that bubbles might be more lean in reality. In terms of hydrodynamic modelling, this seemingly small discrepancy will not be significant, but under reactive conditions with such a reactive oxygen carrier, the void fraction resolved inside the bubble is of great significance since this is where the highly concentrated gas resides. Further study in this direction is recommended.

In order to test the significance of these effects, the simulation was run at a much lower reaction rate and compared against the experimental trend collected for the less reactive ilmenite material [28]. The same model settings that generated the data in Figure 6 were used except for the reaction rate. Reaction kinetics of ilmenite is significantly more complex than that of NiO, however, and no experimental reaction kinetic data is available as of yet. The reaction rate that would adequately represent reactor performance (return quantitatively similar fuel gas conversions) therefore had to be determined by trial and error from the experimental data [28]. In this way, a reaction rate constant 50 times lower than that given in equation (10) was selected. It should be stressed that this numerical experiment was aimed only at testing whether the model could accurately predict an experimental trend under conditions where the inlet effects are expected to play a less significant role. No claims are made that the reaction rate used is representative of the ilmenite material.

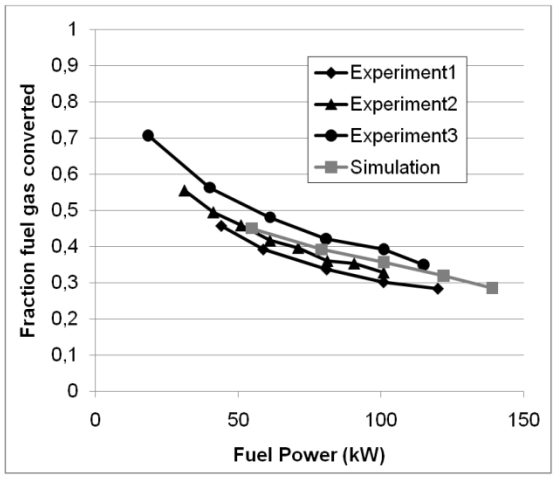

Figure 7: Comparison between experimental measurements for slightly different natural mineral loadings and mixtures [28] and numerical prediction of gas conversion.

As described earlier, the simulation would not be as dependent on the accuracy of the hydrodynamic modelling in the regions of the inlet under this configuration. It is immediately evident from Figure 7 that the model captures the trend much more accurately in this low reactivity case. The model is therefore not as sensitive to the correct description of hydrodynamics any longer and the system generally becomes easier to model. It is also interesting to note that for the 57.4 kW case, a 50 times reduction in

particle reactivity resulted in only a 50% drop in overall system conversion. When expressed on the equivalent reactor scale, a 50 times increase in reaction rate would decrease the reactor size roughly by a factor of 5. This just emphasizes the impact of the mass transfer limitation at play in the high reactivity case. A visual representation of this limitation is given in Figure 8.

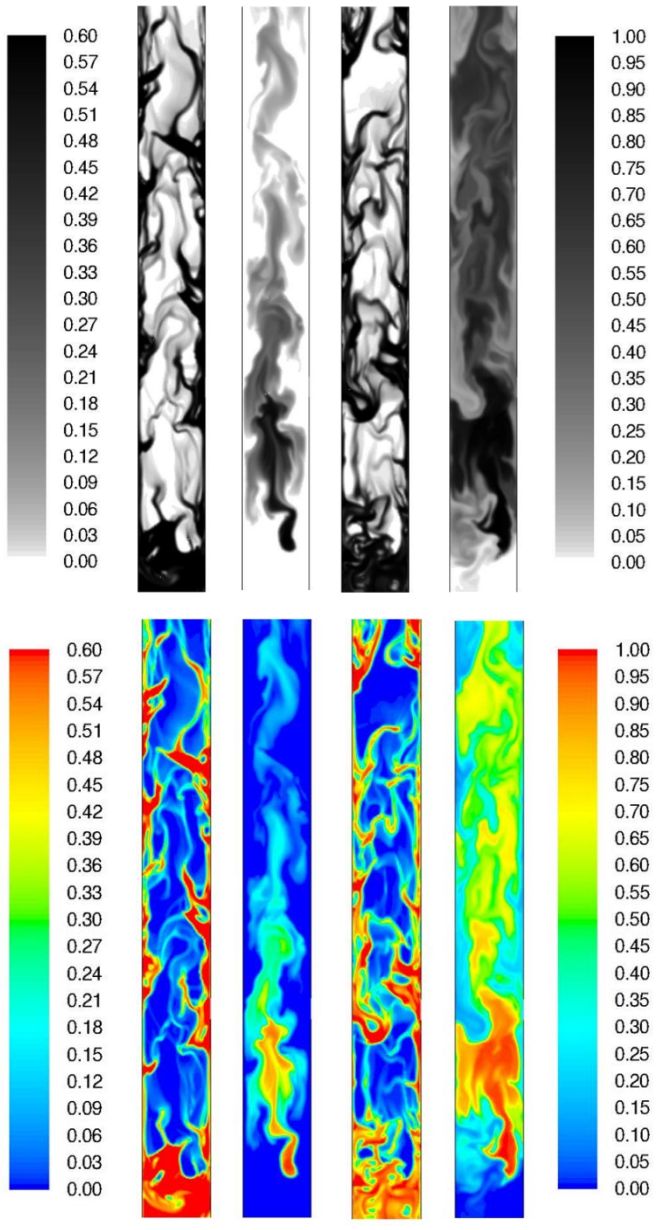

Figure 8: Solids volume fraction and reacting gas contours for the high (two figures on the left) and low (two figures on the right) reactivity cases. The colourmap on the left

represents the solids volume fraction and the one on the right represents the methane mole fraction.

Figure 8 clearly shows no methane in the clusters for the high reactivity case, but a substantial quantity in the low reactivity case. This implies that the large mass of solids residing in the dense clusters is essentially being wasted in the high reactivity case, whereas all the solids partake in the reaction for the case with low reactivity. It is shown that the hydrodynamics of the low reactivity case still has a substantial effect on the fuel distribution, but not as much so as in the high reactivity case.

5.4.3 Discussion on possible dimensional effects

The third candidate for explaining the deviations in Figure 6 is the simulation of 3D experimental results on 2D planar geometries. Due to the core-annular flow regime observed, the bed height in 2D will be over-predicted if the same mass of solids is to be accommodated in the reactor. This would happen because the dense wall regions would account for a smaller amount of the total volume on a 2D plane than in 3D cylinder. The degree of radial solids segregation increases with an increase in fuel power, implying that the over-prediction of bed expansion would increase with increasing flow rates. This over-predicted bed height should lead to over-predictions in reaction rates at higher fuel powers, however, and this is not observed in Figure 6. This implies that, if the bed height was not increasingly over-predicted at higher fuel powers, the trend in Figure 6 might show even greater deviation from the experimental one.

Another possibly significant dimensional effect that could explain the trend in Figure 6 is related to the particle structures gradually changing from slugs/bubbles at lower fuel powers to clusters at higher fuel powers. In 2D, cluster dominated flow would behave substantially differently from the real 3D case since even small clusters are simulated to cause a complete obstruction to the flow field. These falling clusters can therefore be simulated to obstruct a large area of the reactor, leaving only a small opening through which the fuel gas is forced at very high velocities as illustrated in Figure 9. This presents a mechanism by which concentrated fuel gas can slip past the solid particles in a very efficient, but probably unphysical way. In 3D, these small clusters would not block the entire cross sectional area of the reactor and allow for flow to occur in front and behind them as well. This would significantly reduce this highly efficient slippage mechanism.

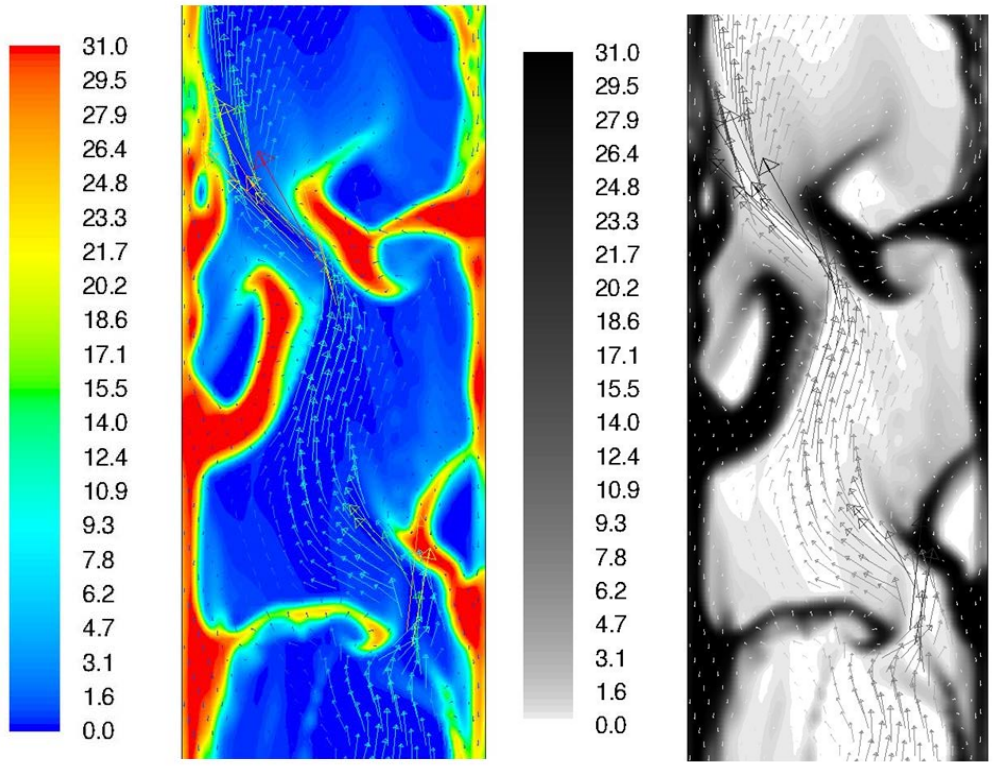

Figure 9: Influence of 2D clusters on the flow field of the gas phase. The colormap indicates the velocity magnitude of the vectors.

Bubble structures, dominating the flow at lower fuel powers, would behave more similarly between 2D and 3D since the reactants trapped within the bubble would be in contact with the entire gas-solid interface both in a 2D and 3D bubble. It can therefore be expected that the reaction rate in cluster dominated flows would significantly increase from 2D to 3D, while that in bubble dominated flows would be more similar. Unfortunately, there is no way in which to numerically test this. The fine-grid 3D simulations required for this purpose are not practically feasible as of yet.

Additionally, the surface area of the gas bubble or particle cluster would be larger in 3D than in 2D because it will be bound in the third dimension as well. Since the correct resolution of the inter-phase boundary has been shown to be the most influential factor in this highly reactive system, any errors in this prediction would have a significant influence on the global conversion rate. Cluster structures are typically substantially smaller than bubble structures, implying that this error will be more significant when considering the larger surface area presented by a cluster dominated flow.

6. Conclusions

Fine-grid, reactive simulations have been completed for the fuel reactor of a pilot scale chemical looping combustion plant operated in the bubbling fluidization regime at the Vienna University of Technology. Grid independence studies have been completed to find that the minimum practical grid resolution is not sufficient to capture the small length scales involved at the concentrated fuel gas injections nozzles used in the experiment. These inlet effects proved to be less influential at higher fuel feed rates where the solids concentration around the inlets was lower. A study on two different inlet configurations also showed a significant effect at low gas feed rates where large solid concentrations were present in the inlet region. The inclusion of gas phase turbulence proved to have a positive effect on the reaction rate. Activation of a turbulence model caused an increase in diffusive species transfer and thereby an increase in the rate at which methane was transported to the gas-emulsion interface.

The simulation could not capture the unexpected increase in methane conversion with an increase in fuel injection rate. This counter-intuitive trend was explained by noting that the reaction rate exhibited by the particles was so rapid that the global reaction behaviour was completely limited by the species transfer in the particle lean regions towards the gas-emulsion interface. The highly concentrated fuel injection mechanism employed in the experiments reduced the degree of gas-emulsion contact, and thereby the reaction rate, by immediately creating clear gas bubbles in the lower fuel power cases.

The general over-prediction of the reaction rate in the lower fuel power cases could be attributed to bubble regions not being sufficiently resolved. Insufficient grid resolution at the inlet is thought to be primarily responsible for the over-prediction of gas-solid contact. It was also shown that the erroneous conversion trend would only worsen if coarser grids are employed. This is a strong indication that the generality of the model is very quickly lost if significant grid dependence effects are present. An analysis of possible dimensional effects was also completed. It was shown that an unphysical fuel gas slippage mechanism is presented in 2D when the flow is cluster dominated. This mechanism was presented by 2D clusters obstructing virtually the entire cross sectional area of the reactor and forcing gas to slip by at high velocities.

Finally, it was found that the model could predict the correct trend when a much less reactive oxygen carrier was used. In this case, reaction rate was the limiting factor and the accurate hydrodynamic resolution of the gas-emulsion interface was of lesser importance. The large influence of the species transfer limitation was also identified in that a 50 times higher reaction rate could only increase the global conversion by a factor of 2-3.

7. Acknowledgement

The authors would like to acknowledge the financial support from SINTEF Materials and Chemistry as well as the Research Council of Norway. The authors also acknowledge the help received from the Vienna University of Technology into building an accurate model of their pilot scale reactor. Finally, the authors

acknowledge the use of the supercomputing facilities at the Norwegian University of Science and Technology for the most expensive simulations carried out in this study.

8. References

[1] Hossain MM, de Lasa HI. Chemical-looping combustion (CLC) for inherent CO2 separations--a review. Chemical Engineering Science. 2008;63(18):4433-51.
[2] Jung J, Gamwo IK. Multiphase CFD-based models for chemical looping combustion process: Fuel reactor modeling. Powder Technology. 2008;183(3):401-9.
[3] Deng Z, Xiao R, Jin B, Song Q. Numerical simulation of chemical looping combustion process with CaSO4 oxygen carrier. International Journal of Greenhouse Gas Control. 2009;3(4):368-75.
[4] Taghipour F, Ellis N, Wong C. Experimental and computational study of gas-solid fluidized bed hydrodynamics. Chemical Engineering Science. 2005;60(24):6857-67.
[5] Ellis N, Xu M, Lim CJ, Cloete S, Johansen ST, Amini S. Effect of Change in Drag Force in Riser Hydrodynamics - Experimental and Numerical Investigations. Submitted to Industrial and Engineering Chemistry Research. 2010.
[6] Pröll T, Kolbitsch P, Bolhàr-Nordenkampf J, Hofbauer H. A novel dual circulating fluidized bed system for chemical looping processes. AIChE Journal. 2009;55(12):3255-66.
[7] Wang J, Ge W, Li J. Eulerian simulation of heterogeneous gas-solid flows in CFB risers: EMMS-based sub-grid scale model with a revised cluster description. Chemical Engineering Science. 2008;63(6):1553-71.
[8] Wang W, Li J. Simulation of gas-solid two-phase flow by a multi-scale CFD approach-of the EMMS model to the sub-grid level. Chemical Engineering Science. 2007;62(1-2):208-31.
[9] Benyahia S. On the effect of subgrid drag closures. Industrial and Engineering Chemistry Research. 2010;49:5122-31.
[10] Andrews AT, Loezos PN, Sundaresan S. Coarse-grid simulation of gas-particle flows in vertical risers. Industrial and Engineering Chemistry Research. 2005;44(16):6022-37.
[11] Lu H, Wang S, He Y, Ding J, Liu G, Hao Z. Numerical simulation of flow behavior of particles and clusters in riser using two granular temperatures. Powder Technology. 2008;182(2):282-93.
[12] Cloete S, Amini S, Johansen ST. On the Effect of Cluster Resolution in Riser Flows on Momentum and Reaction Kinetic Interaction. Submitted to Powder Technology. 2010.
[13] Gidaspow D, Bezburuah R, Ding J. Hydrodynamics of Circulating Fluidized Beds, Kinetic Theory Approach. *7th Engineering Foundation Conference on Fluidization* 1992:75-82.
[14] Syamlal M, Rogers W, O'Brien TJ. MFIX Documentation: Volume 1, Theory Guide. Springfield: National Technical Information Service 1993.
[15] Wen CY, Yu YH. Mechanics of Fluidization. Chemical Engineering Progress Symposium Series. 1966;62:100-11.
[16] Smagorinsky J. General Circulation Experiments with the Primitive Equations. I. The Basic Experiment. Monthly Weather Review. 1963;91:99-164.
[17] Murakami S, Mochida A. On turbulent vortex shedding flow past 2D square cylinder predicted by CFD. Journal of Wind Engineering and Industrial Aerodynamics. 1995;54-55:191-211.
[18] Bruno L, Khris S. The validity of 2D numerical simulations of vortical structures around a bridge deck. Mathematical and Computer Modelling. 2003;37:795-828.

[19] Lun CKK, Savage SB, Jeffrey DJ, Chepurniy N. Kinetic Theories for Granular Flow: Inelastic Particles in Couette Flow and Slightly Inerlastic Particles in a General Flow Field. Journal of Fluid Mechanics. 1984;140:223-56.
[20] Schaeffer DG. Instability in the Evolution Equations Describing Incompressible Granular Flow. Journal of Differential Equations. 1987;66:19-50.
[21] Ogawa SU, A.; Oshima, N. On the Equation of Fully Fluidized Granular Materials. Journal of Applied Mathematics and Physics. 1980;31:483.
[22] Levenspiel O. Chemical Reaction Engineering. 3 ed: John Wiley & Sons 1999.
[23] Abad A, Adanez J, Garcia-Labiano F, de Diego L, Gayan P, Kolbitsch P, et al. CLC Modelling: the Fuel-Reactor at Fast Fluidization - Conversion of CH4 using a NiO-based Oxygen-Carrier in a 120 kW Unit. *1st International Conference on Chemical Looping*. Lyon, France 2010.
[24] Johnson PC, Jackson R. Frictional-Collisional Contitutive Relations for Granular Materials, with Application to Plane Shearing. Journal of Fluid Mechanics. 1987;176:67-93.
[25] Patankar S. Numerical Heat Transfer and Fluid Flow: Hemisphere Publishing Corporation 1980.
[26] Leonard BP, Mokhtari S. ULTRA-SHARP Nonoscillatory Convection Schemes for High-Speed Steady Multidimensional Flow. NASA TM 1-2568 (ICOMP-90-12); 1990; NASA Lewis Research Center; 1990.
[27] Cloete S, Amini S, Johansen ST. A fine Resolution Parametric Study on the Numerical Simualtion of Riser Flows. Powder Technology. 2010;In print.
[28] Pröll T, Mayer K, Bolhàr-Nordenkampf J, Kolbitsch P, Mattisson T, Lyngfelt A, et al. Natural minerals as oxygen carriers for chemical looping combustion in a dual circulating fluidized bed system. Energy Procedia. 2009;1(1):27-34.
[29] Bi HT, Grace JR. Flow regime diagrams for gas-solid fluidization and upward transport. International Journal of Multiphase Flow. 1995;21(6):1229-36.
[30] Zhu H, Zhu J, Li G, Li F. Detailed measurements of flow structure inside a dense gas-solids fluidized bed. Powder Technology. 2008;180(3):339-49.